Journal of Engineering Science and Technology
Vol. 14, No. 2 (2019) 763 - 783

DESIGN OF FRACTIONAL ORDER PID CONTROLLER FOR AGC LOOP IN A DEREGULATED POWER SYSTEM WITH RFB AND IPFC UNITS

V. SURESH BABU[1,*], K. SHANMUKHA SUNDAR[2]

[1]National Power Training Institute/PSTI, Ministry of Power,
Government of India, Bengaluru, Karnataka, India
[2]Department of EEE, Dayananda Sagar College of Engineering,
Bengaluru, Karnataka, India
*Corresponding Author: sureshbabu27@gmail.com

Abstract

This article presents the Fractional Order Proportional-Integral-Derivative (FOPID) controller for Automatic Generation Control (AGC) of an interconnected two-area wind-thermal deregulated power system. A FOPID controller is a classical PID except for its derivative and integral orders are fractional numbers in place of being integers. The control parameters of FOPID controller are tuned using Lightning Search Algorithm (LSA) and its performance is compared with Proportional-Integral (PI), Pseudo-Derivative Feedback with Feed-forward controller (PDFF) and Proportional-Integral-Derivative with Derivative Filter (PIDF) controllers based AGC. Further, to improve the AGC performance, combination Redox Flow Batteries (RFB) and Interline Power Flow Controller (IPFC) are included in its control area. The implementation of RFB-IPFC combination arrests the initial fall in frequency as well as the tie line power deviations after a sudden load disturbance. The simulation results reveal that the supremacy of projected FOPID controller, the dynamic performance of AGC loop have improved in terms of less peak deviation and settling time of area frequencies and tie-line power in different transactions of the deregulated power system. In large load disturbance situation, RFB-IPFC unit connected in any area and tie-line respectively responds much faster than the conventional governor action of the wind-thermal system. In order to damp out the system oscillations, the RFB unit reacts during the starting position of the load disturbance by injecting the stored energy in it. The frequency oscillation and tie-line power deviations in the control areas are reduced and the settling time is also improved when the RFB-IPFC combination participates in the frequency regulation along with the conventional generators. Thus, coordinated operation of RFB-IPFC in AGC loop could enhance the system performance.

Keywords: AGC, FOPID controller, IPFC, LSA, PDFF controller, PIDF controller, RFB.

1. Introduction

The deregulated power system, Automatic Generation Control (AGC) is an important control problem in an interconnected power system. The most important objectives of the AGC is to maintain system frequency as well as tie-line power deviations within permissible limit by regulating the output power of each generator at agreed levels in response to continuously-changing load demand [1]. The AGC action is directed by the Area Control Error (ACE), which is a role of system frequency and tie line power flows. Elgerd [2] proposed that as the ACE is focused on zero by the AGC, both frequency and tie-line power errors will be put on to zero. At the present time, the conventional power system has been changed to a deregulated environment. A deregulated power system comprises of generation companies (Gencos), distribution companies (Discos), transmission companies (Transco) and Independent Contract Administrator (ICA).

In such a new scenario, Discos can autonomously make an agreement with Gencos for delivery power to meet the demand of the consumer. An ICA is a self-governing agent that manages all the transactions alleged between Discos and Gencos. A Disco Participation Matrix (DPM) is used for a hallucination of bonds between Gencos and Discos [3-6]. In the current conservative scenario, hydro and thermal units are the major power producer units. The hydro plant transfer function offers non-minimum phase characteristics that are different from the thermal plants. Due to certain drawbacks of carbon emission, it is necessary to incorporate renewable sources of energy like wind energy. Wind power plants have been integrated into a grid as they are used as peak load plants to preserve the reliability of supply. The control of frequency becomes difficult and hence, challenging, in the presence of a wind farm due to the discontinuous nature of wind speed. In addition, based on studies by Saha and Saikia [7], due to the boundaries of conventional sources, it is necessary to make use of non-conventional sources to study the AGC problem.

Hingorani and Gyugyi [8] explained that in an interconnected area, inter-area oscillations may occur, which results in severe frequency deviation. Flexible AC Transmission System (FACTS) devices are also used to damp out these oscillations. The most versatile FACTS devices such as Unified Power Flow Controller (UPFC) and Interline Power Flow Controller (IPFC), which are connected in series with the tie-lines to control the power flow. However, IPFC is pretty for compensating multi-line systems from an economical point of outlook [9]. IPFC can reimburse each transmission line independently so that the power optimization of the overall system can be obtained in the form of suitable power transfer from over-loaded lines to under loaded lines [10]. In view of the above, an IPFC is considered in the present paper.

In addition, energy storage devices such as Capacitive Energy Storage (CES), Superconductor Magnetic Energy Storage Systems (SMES) and Redox Flow Batteries (RFB) have improved the power transfer capability and power management of the interconnected power system. Redox Flow Batteries (RFB) is an energetic power source, which can be necessary not only as a rapid energy compensation device for power utilization of huge loads, however, also as a stabilizer of frequency oscillations [11]. The RFB has been compensated an accumulation of load and could maintain power quality for deregulated power supplies. However, due to the economic motive, it is not feasible to rest RFB in each area. When IPFC and RFB are present in the system, they should operate in a

coordinated manner so as to control the network conditions in a very rapid and cost-effective manner.

On the other hand, for the secondary control of AGC, several classical controller structures such as Integral (I), Proportional-Integral (PI), Proportional-Integral-Derivative (PID), and Integral Derivative (ID) have been used and their performance has been compared for an AGC system and it is established that PID controller give superior performance over the other controllers [12]. However, the main disadvantages of the parallel PID controllers are the possessions of proportional and derivative kick, which grades in abrupt spikes and gratuitous overshoot. In a PID controller, the derivative mode recovers stability of the system and enhances the speed of the controller response, however, it makes the plant to draw a huge amount of control input. In addition, any noise in the control input signal will outcome in large plant input signals distortion, which often leads to complications in practical applications. The practical solution to these problems is to put the first filter on the imitative term and tune its pole so that the distortion due to the noise does not occur since it eases high-frequency noise [13].

A Proportional Integral Derivative with derivative Filter (PIDF) controllers are intended and realized for the AGC under deregulated atmosphere problems. Pseudo-Derivative Feedback with Feed-Forward Controller (PDFF) adds the forward gain K_{FR}, which allows the user to raise the integral gain and provides a much better response than the aforesaid controllers. The performance of PID controllers can be improved by using the fractional calculus. In Fractional Order (FO) controllers, the order of integral and derivative terms is not an integer [14]. The main advantage associated with FO controllers is flexibility in controlling purpose, which helps to design a robust control system. FO controllers have excellent capability of handling parameter uncertainty, elimination of steady-state error and better stability [15]. Fractional Order Proportional Integral Derivative (FOPID) controllers are being used in different fields of engineering, such as stabilizing fractional order time-delay systems, automatic voltage regulator system, etc.

The fractional order PID (FOPID) controller is the extension of the conventional PID controller based on fractional calculus. In FOPID, besides proportional (K_P), integral (K_I) and derivative (K_D) gains, the controller has two more parameters, integral order (λ) and derivative order (μ) as design specifications, which provide greater flexibility in controller design [16]. In many cases, fractional calculus can be applied to improve the stability and response of such a system, through the use of non-integer order integrals and derivatives in place of the typical first order ones. There are many systems in reality, which are better described and controlled by FO dynamic equations. A few controllers such as PDFF, PIDF and FOPID have considered in this study of AGC loop for a two-area wind-thermal interconnected power system.

Several optimization techniques plays an important role to find the optimal controller parameters such as Particle Swarm Optimization (PSO), Genetic Algorithm (GA), Biogeography-Based Optimization (BBO), Krill Herd Algorithm (KHA), Teaching Learning Based Optimization (TLBO) and Bacterial Foraging Optimization (BFO) algorithm have been planned to resolve the control parameters of a several standard controllers to solve the AGC problem [17-22]. A more recent powerful meta-heuristic algorithm called Lightning Search Algorithm (LSA) is a powerful and flexible optimization technique that was inspired by the natural

phenomenon of lightning [23]. The advantages of this algorithm are to be utilized for optimization of PDFF, PIDF and FOPID controller gains of AGC loop for two-area wind-thermal interconnected deregulated power system without and with IPFC and RFB units for different transactions. The rest of the paper is organized as follows: (a) to design a two-area wind-thermal deregulated power system having different capacities (b) to design and optimized PDFF, PIDF and FOPID controller using LSA and analyse the dynamic performance for AGC loop in deregulated power system (c) to study the effect of IPFC and RFB in AGC studies (d) to test the effectiveness of proposed controllers in a two-area wind-thermal deregulated power system with IPFC and RFB.

2. Modelling of two-area wind-thermal deregulated power system

In the deregulated power system, Discos in every area can bond with Gencos in its own or other areas. There are a number of Gencos and Discos within the deregulated power system and a Disco has the liberty to cover a contract with any Genco for a contract of power. According to Donde et al. [3], such transactions are called bilateral transactions. All the transactions have to be comprehensible through an impartial entity called an ICA. In this study, the two-area wind-thermal deregulated power system is considered in which, each area has two Gencos and two Discos is shown in Fig. 1. In the recent background, Discos may contract power from any Gencos and ICA has to supervise these contracts. DPM is a matrix in which, the number of rows is equal to the number of Gencos and the number of columns is equal to the number of Discos in the system. Each entry in this matrix can be considered for the portion of a total load contracted by a Disco towards a Genco. The sum of all the entries in a column DPM is unity. From Fig. 1, let $Genco_1$, $Genco_2$, $Disco_1$, $Disco_2$ be in area 1 and $Genco_3$, $Genco_4$, $Disco_3$, $Disco_4$ be in area 2. The corresponding DPM is given as follows:

$$DPM = \begin{bmatrix} cpf_{11} & cpf_{12} & cpf_{13} & cpf_{14} \\ cpf_{21} & cpf_{22} & cpf_{23} & cpf_{24} \\ cpf_{31} & cpf_{32} & cpf_{33} & cpf_{34} \\ cpf_{41} & cpf_{42} & cpf_{43} & cpf_{44} \end{bmatrix} \tag{1}$$

where *cpf* represents "contract participation factor", i.e., p.u. MW load of a corresponding Disco. Donde et al. [3] given the scheduled steady state power flow on the tie-line.

$$\Delta P_{Tie\ 12}^{scheduled} = \sum_{i=1}^{2}\sum_{j=3}^{4} cpf_{ij}\,\Delta P_{Lj} - \sum_{i=3}^{4}\sum_{j=1}^{2} cpf_{ij}\,\Delta P_{Lj} \tag{2}$$

The actual tie-line power is given as:

$$\Delta P_{Tie\ 12}^{actual} = \frac{2\pi T_{12}}{s}(\Delta F_1 - \Delta F_2) \tag{3}$$

Donde et al. [3] given at any time, the tie-line power error.

$$\Delta P_{Tie\ 12}^{Error} = \Delta P_{Tie\ 12}^{actual} - \Delta P_{Tie\ 12}^{scheduled} \tag{4}$$

$\Delta P_{Tie\ 12}^{Error}$, vanishes in the steady as the actual tie-line power flow reaches the scheduled power flow. This error signal is used to generate the respective Area Control Error (ACE) signals as in the traditional scenario [3].

$$ACE_1 = \beta_1 \Delta F_1 + \Delta P_{Tie12}^{Error} \quad (5)$$

$$ACE_2 = \beta_2 \Delta F_2 + a_{12} \Delta P_{Tie12}^{Error} \quad (6)$$

The generation of each Genco must footpath the contracted demands of Discos in steady state. The desire total power generation of i[th] Genco in terms of DPM entries can be calculated as:

$$\Delta P_{mi} = \sum_{j=1}^{4} cpf_{ij}\, \Delta P_{Lj} \quad (7)$$

As there are two Gencos in each area, the ACE signal has to be dispersed among them in proportion to their participation in the AGC. Coefficients that distribute ACE to Gencos are termed as ACE Participation Factors (apfs). In a given control area, the sum of participation factors is equal to 1. Hence, apf_{11}, apf_{12} are considered as ACE participation factor in area 1 and apf_{21}, apf_{22} are in area 2.

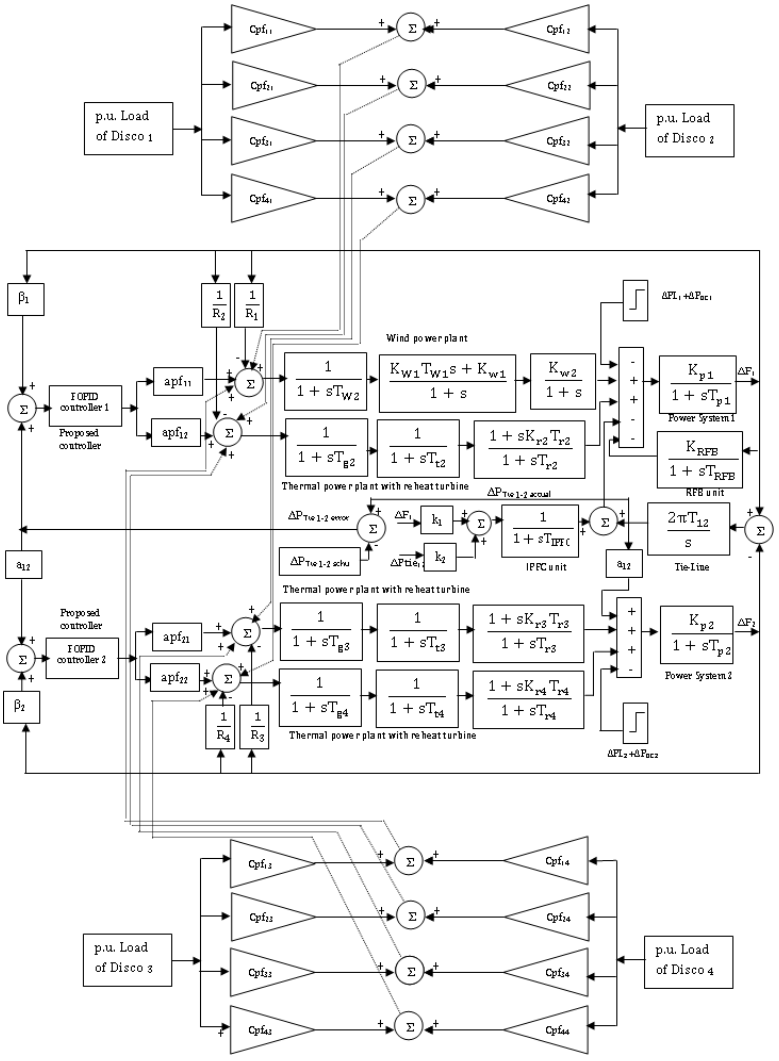

Fig. 1. Transfer function model of two-area wind-thermal power system with IPFC and RFB units in deregulated environment.

3. Design of PDFF, PIDF and FOPID controller using LSA

3.1. Controller structure of PDFF controller

Figure 2 shows a PDFF controller. Like the PI controller, it has an integral gain (K_I) and a proportional gain (K_P). The PDFF adds the gain K_{FR}, which allows the user to raise the integral gain in some applications. When an application requires the maximum responsiveness and do not need much integral gain and set K_{FR} high. When the application requires maximum low-frequency stiffness, set K_{FR} low, this allows much higher integral gain without inducing overshoot. Unfortunately, it also makes the system slower in responding to the command. The majority of motion control applications are in the middle and K_{FR} = 65% usually gives good results. In this study, K_{FR} set to 0.65 then K_P and K_I values are tuned using the LSA technique.

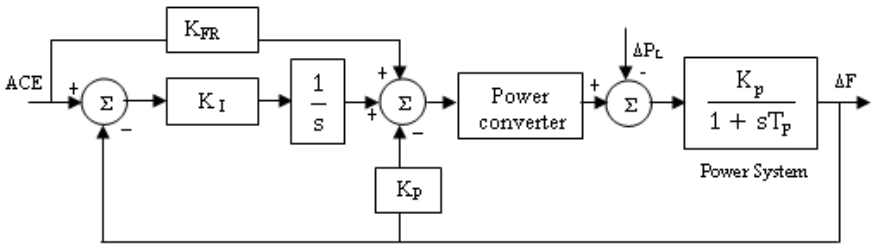

Fig. 2. Block diagram for PDFF control.

3.2. Control structure of PIDF controller

The structure of PID controller with derivative filter is shown in Fig. 3. Where K_P, K_I and K_D are the proportional, integral and derivative gains respectively and N is the derivative filter coefficient. The transfer function of the proposed PIDF controller is given by:

$$T(s) = K_P + \frac{K_I}{s} + K_D\left(\frac{N*s}{s+N}\right) \tag{8}$$

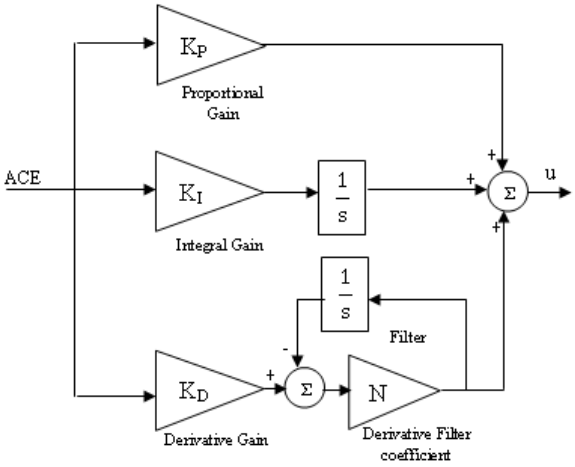

Fig. 3. Block diagram for PIDF controller.

3.3. Controller structure of FOPID controller

The block diagram of Fractional Order PID (FOPID) controller, referred to as $PI^{\lambda}D^{\mu}$ controller is shown in Fig. 4. In FOPID controller, in addition to K_P, K_I and K_D there are two more parameters λ and μ, the integral and derivative orders respectively. The transfer function of the proposed FOPID controller is given by:

$$T(s) = K_P + \frac{K_I}{s^{\lambda}} + K_D s^{\mu} \qquad \lambda, \mu > 0 \tag{9}$$

If $\lambda = 0$ and $\mu = 0$, then it is just only a proportional (P) controller, If $\lambda = 0$ and $\mu = 1$, then it becomes a proportional-derivative (PD) controller, If $\lambda = 1$ and $\mu = 0$, then it becomes a proportional-integral (PI) controller and If $\lambda = 1$ and $\mu = 1$, then it becomes integer PID. These integer order controllers are represented as points in λ - μ plane as shown in Fig. 5(a). Therefore, FOPID controller generalizes the PID controller and expands it from point to entire λ - μ plane as shown in Fig. 5(b), thus, offering a much wider selection of tuning parameters thereby, more flexibility in the controller design leading to more accurate control [16]. The LSA techniques are used to determine the optimal constraints of PDFF, PIDF and FOPID controllers with the objective to minimize Integral square of area control error, which can be formulated in the following manner:

$$J = \int_0^{t_{sim}} (\Delta F_1^2 + \Delta F_2^2 + \Delta P_{tie}^2)\, dt \tag{10}$$

The problem constraints are the proposed controller parameter bounds. Therefore, the design problem can be formulated as,

$$Minimize\ J \tag{11}$$

Subject to

$$K_P^{min} \le K_P \le K_P^{max}, K_I^{min} \le K_I \le K_I^{max}, K_D^{min} \le K_D \le K_D^{max}, K_{FR}^{min} \le K_{FR} \le K_{FR}^{max}, N^{min} \le N \le N^{max}, \lambda^{min} \le \lambda \le \lambda^{max}, \mu^{min} \le \mu \le \mu^{max}, \tag{12}$$

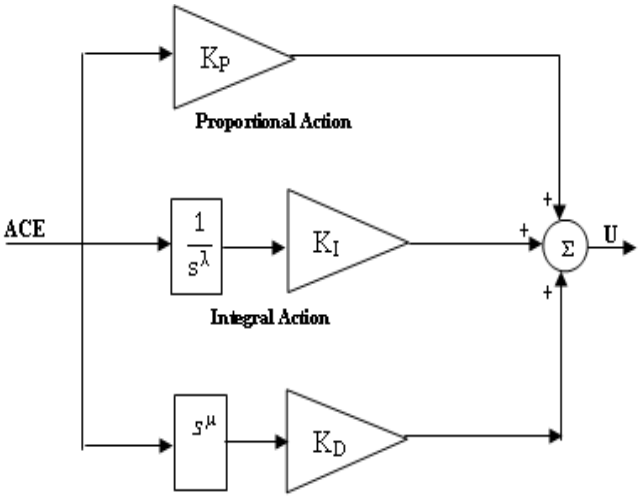

Fig. 4. Block diagram for FOPID controller.

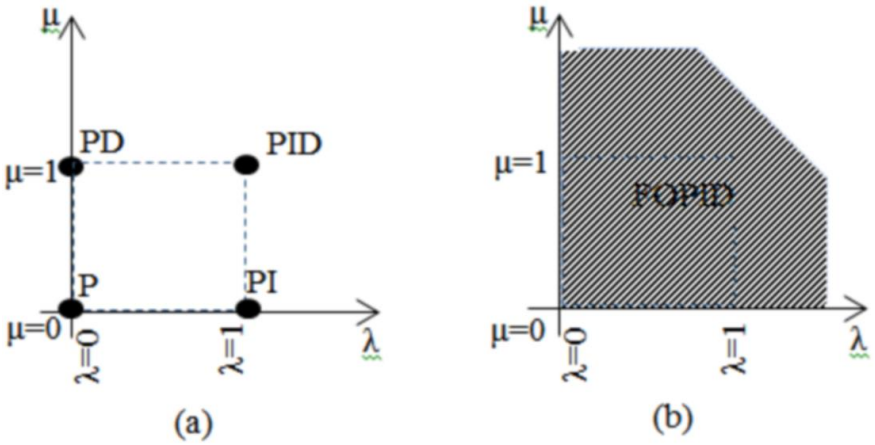

Fig. 5(a) Integer order P/PI/PD/PID controllers, (b) Fractional order PID controller.

3.4. Lightning search algorithm

LSA is a natural phenomenon based on a novel meta-heuristic algorithm. It is based on the lightning mechanism, which involves the propagation of step leader [23, 24]. Some of the molecules of water condensed from a thundercloud split in random directions, known as projectiles. It is considered that the fast particles called projectiles form the binary tree structure of the step leader. The initial population size of the algorithm is represented by these projectiles. The velocity of the projectile is shown in Eq. (13).

$$v_p = \left[1 - \left(\frac{1}{\sqrt{1-\left(\frac{v_0}{c}\right)^2-\left(\frac{sF_i}{mc^2}\right)}}\right)^{-2}\right]^{-1/2} \tag{13}$$

where v_0 is the initial velocity of the projectile, m is the mass of the projectile, F_i is the constant ionisation rate, c is the speed of light and s is the length of the path travelled. Thus, the projectile has less potential to ionise or explore a large space if the mass is less and travelled path is long.

Hence, the relative energy of the step leader controls the exploration and exploitation of the algorithm. An important property of projectile is forking, which improves the bad solution of the population and if it is not so one of the channels at the forking point is lighted up to keep the population size. In this algorithm, three types of projectiles are introduced to represent the whole step leader movement. These are transition projectiles, which construct the population of first step leader, space projectile, which try to attain the best position and lead projectile, which represents the best position among all population. Since the transition projectiles are ejected in a random direction, a random number can represent it from uniform probability distribution function, which is given by Eq. (14).

$$f(x^T) = \begin{Bmatrix} \frac{1}{b-a}; & a \le x^T \le b \\ 0 \quad ; & x < a, x^T > b \end{Bmatrix} \tag{14}$$

where x^T is the random number that gives the solution or the initial tip energy of step leader *i*, *a* and *b* are the lower and upper boundaries of the solution space. After evolving the *N* step leader tips, it will move by ionising the surrounding area of the old leader using energetic projectiles in the next step. The position of the space projectile can be obtained from the probability density function of exponential distribution as shown in (15)

$$f(x^s) = \begin{cases} \frac{1}{\mu} e^{-x^{si\mu}}; & a < x^T < b \\ 0 \quad ; & x^{\ s} \leq 0 \end{cases} \tag{15}$$

where, μ is the shaping parameter, which determines the space projectile position or direction in the next step. For a particular space projectile, μ_i is considered as the distance between the lead projectile and space projectile in the algorithm. The position of a particular space projectile is given by (16)

$$P_{i-new}^s = P_i^s \mp \exp\ rand_i\ (\mu_i) \tag{16}$$

If the projectile energy is not greater than the step leader, the new position of the space projectile does not ensure propagation of stepped leader to expand the channel. If it is not so, it will become lead projectile. The normal probability distribution function of the lead projectile with scale parameter σ is given by (17)

$$f(x^L) = \frac{1}{\sigma\sqrt{2\pi}} e^{-\left(x^L-\mu\right)^2/2\sigma^2} \tag{17}$$

In LSA, the best solution can be obtained as a shape parameter for space projectile and scale parameter decreases exponentially. The position of the lead projectile is expressed in (18).

$$P_{new}^L = P^L + norm\ rand_i(\mu_L, \sigma_L) \tag{18}$$

If the new position of the lead projectile gives a good solution, then the step leader is extended and the lead projectile position is updated. Thus, exploitation and exploration are performed by space and lead projectiles to find the optimum solution. The exploration is represented by exponential random behaviour of the space projectile and exploitation process is controlled by a lead projectile with a random search. The control parameters of LSA are population size, maximum iteration and channel time. In this paper, population size, maximum iteration and channel time are considered as 100, 100 and 20, respectively.

4. System modelling for control design of IPFC and RFB

The combined action between IPFC and RFB units are found to be superior to that of the governor system in terms of the faster response against the frequency fluctuations. The linearized reduction model test system with RFB and IPFC units for the control design are shown in Fig. 6. Where the forceful of governor system is eradicated by setting the mechanical inputs as constant since the response of governor is much slower than that of RFB and IPFC units. From the objective outlook aim, it is noted that the RFB unit is fitted in area 1 and IPFC unit are located in the tie-line, which is capable in successful to alleviate inertia and inter-area mode oscillations respectively. The RFB is modelled as an active power source with gain constant K_{HES} and time constant T_{HES}. The IPFC is modelled as a tie-line power flow controller with a time constant $T_{IPFC.}$ From Fig. 6, the state equations are derived as follows.

$$\begin{bmatrix} \Delta\dot{F}_1 \\ \Delta\dot{P}_{T12} \\ \Delta\dot{F}_2 \end{bmatrix} = \begin{bmatrix} -1/T_{p1} & -k_{p1}/T_{p1} & 0 \\ 2\pi T_{12} & 0 & -2\pi T_{12} \\ 0 & a_{12}\,k_{p2}/T_{p2} & -1/T_{p2} \end{bmatrix} \begin{bmatrix} \Delta F_1 \\ \Delta P_{T12} \\ \Delta F_2 \end{bmatrix} + \begin{bmatrix} k_{p1}/T_{p1} & -k_{p1}/T_{p1} \\ 0 & 0 \\ 0 & a_{12}\,k_{p2}/T_{p2} \end{bmatrix} \begin{bmatrix} \Delta P_{RFB} \\ \Delta P_{IPFC} \end{bmatrix} \quad (19)$$

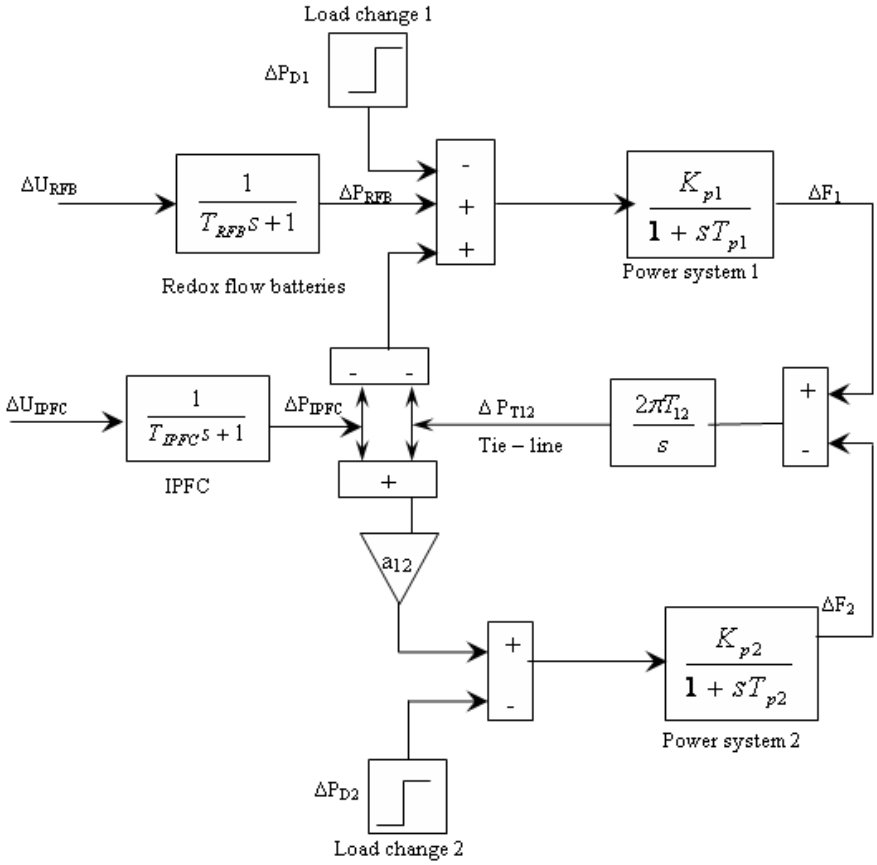

Fig. 6. Linearized reduction model for control design.

Control design of Redox Flow Batteries unit

The design process starts with the reduction of two-area systems into one area, which represents the Inertia centre mode of the overall system. The controller of RFB is considered in the equivalent one area system to reduce the frequency deviation of the centre of inertia. The equivalent system is derived by assuming the synchronizing coefficient T_{12} to be large. From the state equation of ΔP_{T12} in Eq. (19).

$$\frac{\Delta\dot{P}_{T12}}{2\pi T_{12}} = \Delta F_1 - \Delta F_2 \quad (20)$$

Let us assume the synchronous coefficient (T_{12}) is infinity, then Eq. (20) becomes $\Delta F_1 = \Delta F_2$. Expanding in Eq. (19), $\Delta\dot{F}_1$ and $\Delta\dot{F}_2$ multiplying by T_{p1}/k_{p1} and $T_{p2}/a_{12}k_{p2}$ respectively

$$(T_{p1}/k_{p1})\,\Delta\dot{F}_1 = -(1/k_{p1})\Delta F_1 - \Delta P_{T12} + \Delta P_{RFB} - \Delta P_{IPFC} \quad (21)$$

$$(T_{p2}/a_{12}k_{p2})\,\Delta\dot{F}_2 = -(1/a_{12}k_{p2})\Delta F_2 + \Delta P_{T12} + \Delta P_{IPFC} \quad (22)$$

Sub $\Delta F_1 = \Delta F_2 = \Delta F$ and summing Eqs. (21) and (22) we get:

$$\Delta\dot{F} = \left(-1/k_{p1} - (1/a_{12}k_{p2})\right)/\left((T_{p1}/k_{p1}) + (T_{p2}/a_{12}k_{p2})\right) + \left(1/\left((T_{p1}/k_{p1}) + (T_{p2}/a_{12}k_{p2})\right)\right)\Delta P_{RFB} + C\Delta P_D \quad (23)$$

The load change in this system ΔP_D is additionally considered, where C is constant, here the control $\Delta P_{RFB} = -K_{RFB}\,\Delta F$ is applied then.

$$\Delta F = \frac{C}{s + A + K_{RFB}\,B}\,\Delta P_D \quad (24)$$

where $A = \left(-1/k_{p1} - (1/a_{12}k_{p2})\right)/\left((T_{p1}/k_{p1}) + (T_{p2}/a_{12}k_{p2})\right)$

$B = 1/\left((T_{p1}/k_{p1}) + (T_{p2}/a_{12}k_{p2})\right)$;

The C- is the proportionality between change in frequency and change in load demand. In (24), the final values with $K_{RFB} = 0$ and $K_{RFB} \neq 0$ are C/A and C/(A+K_{RFB} B) respectively, therefore, the percent reduction is represented by:

$$(C/A + K_{RFB}\ B)/(C/A) = R/100 \quad (25)$$

The control gain of RFB unit is expressed as:

$$K_{RFB} = (A/BR) * (100 - R) \quad (26)$$

Control design of Interline Power Flow Controller unit.

The controller for the IPFC is intended to improve the damping of the inter-area mode. In order to extract the inter-area mode from the system Eq. (19), the concept of overlapping decompositions is applied. Then, one subsystem, which preserves the inter-area mode, is represented by Eq. (27).

$$\begin{bmatrix} \Delta\dot{F}_1 \\ \Delta P_{T12} \end{bmatrix} = \begin{bmatrix} -1/T_{p1} & -k_{p1}/T_{p1} \\ 2\pi T_{12} & 0 \end{bmatrix} \begin{bmatrix} \Delta F_1 \\ \Delta P_{T12} \end{bmatrix} + \begin{bmatrix} -k_{p1}/T_{p1} \\ 0 \end{bmatrix} [\Delta P_{IPFC}] \quad (27)$$

The control principle of the IPFC is to dampness the peak rate of frequency deviation in area 1 after a rapid varies in the load demand. Since the system Eq. (27) is the second order oscillation system, the overshoot *Mp (new)* can be specified for the control design. *Mp* (new) is given as a function of the damping ratio by Eq. 28.

$$M_{P\,new} = e^{\left(-\pi\delta/\sqrt{1-\delta^2}\right)} \quad (28)$$

The real and imaginary parts of the eigenvalue after the control are expressed as $\alpha_s = \delta\,\omega_n$ and $\beta_s = \omega_{n\sqrt{1-\delta^2}}$. Where w_n is the undamped natural frequency, by specifying *Mp* and assuming $\beta_s = \beta$, the desired pair of the eigenvalue is fixed. As a result, the eigenvalue assignment method derives to feedback scheme as Eq. 29.

$$\Delta P_{IPFC} = -k_1\Delta F_1 - k_2\Delta P_{T12} \quad (29)$$

5. Simulation Results and Observations

5.1. Dynamic output responses of AGC loop with proposed controller

Scenario 1. Poolco based transaction

In this scenario, Gencos participate only in the load following control of their areas. It is assumed that a large step load of 0.2 p.u. MW is demanded by each Disco in area 1. Assume that a case of Poolco based contracts between Dicos and available Gencos is simulated based on the following Disco Participation Matrix (DPM) referring to Eq. (1) is considered as:

$$DPM_1 = \begin{bmatrix} 0.5 & 0.5 & 0.0 & 0.0 \\ 0.5 & 0.5 & 0.0 & 0.0 \\ 0.0 & 0.0 & 0.0 & 0.0 \\ 0.0 & 0.0 & 0.0 & 0.0 \end{bmatrix} \tag{30}$$

Disco$_1$ and *Disco*$_2$ demand identically from their local Gencos, viz., *Genco*$_1$ and *Genco*$_2$. Therefore, $cpf_{11} = cpf_{12} = 0.5$ and $cpf_{21} = cpf_{22} = 0.5$. In this test system, it consists of two Gencos and two Discos in each area. The wind and thermal units are Gencos in area-1 and two thermal units as Gencos in area-2. The nominal parameters are given in *Appendix* 1.

The proposed controller is tuned using with PSO, BFO and LSA technique and implemented two-area interconnected wind-thermal deregulated power system for different transactions.

In Fig. 7, shows comparative transient performances of the thermal-diesel power system for given load perturbation. From Fig. 7, it can be observed that the oscillations in the area frequencies and tie-line power deviations have decreased to a considerable extent with LSA tuned FOPID controller when compared the output responses obtained using PSO, BFO technique based FOPID controller.

It can be inferred that the LSA tuned FOPID controller gives better results in terms of settling time, overshoot and undershoot. Simulation results reveal the accuracy of finding the best solution and convergence speed performance of the proposed algorithm is significantly better compared to those achieved by the existing algorithms. Then the performance of LSA tuned FOPID, PI, PDFF and PIDF are analysing for the test systems under Poolco based transactions and bilateral transactions.

The optimum control parameters of PI, PDFF, PIDF and FOPID controllers are shown in Table 1 and the comparative system dynamic response of all controllers is shown in Fig. 8. The peak over/undershoot and settling time of frequency deviation of both areas and tie-line power deviation with a different controller are tabulated in Table 2. From Table 2 and Fig. 8, it can be observed that the proposed FOPID controller have better dynamic responses as compared with PI, PDFF and PIDF controller in terms of peak over/undershoot and settling time of frequency deviation both areas and tie-line power oscillations in AGC loop.

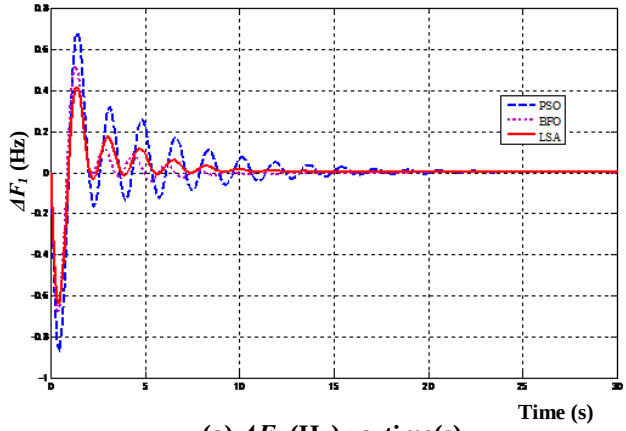

(a) ΔF_1 (Hz) vs. time(s).

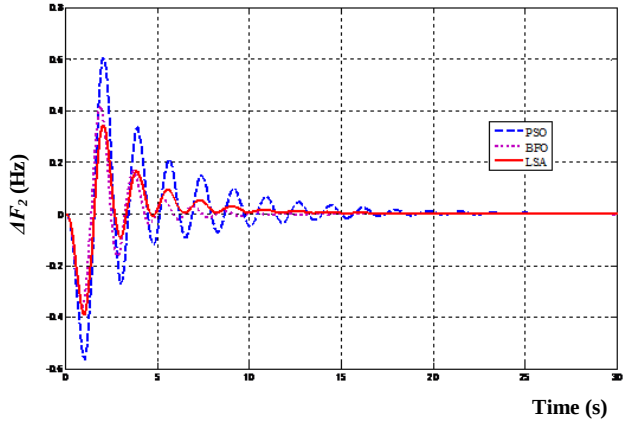

(b) ΔF_2 (Hz) vs. time (s).

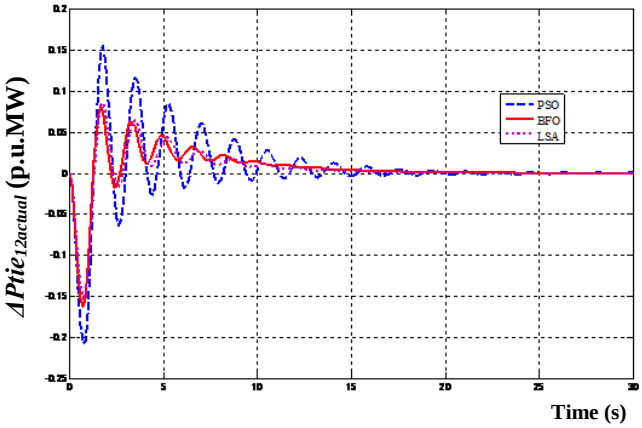

(c) $\Delta Ptie_{12,\ actual}$ (p.u., MW) vs. time (s).

Fig. 7. Dynamic responses of the frequency deviations, tie- line power deviations for a two-area wind-thermal system with FOPID controller using different optimization algorithm under Poolco based transactions.

Table 1. Optimum values of control parameters of various controllers under different types transactions.

Controller	Gain/ parameters	Poolco based transactions		Bilateral based transactions	
		Area-1	Area-2	Area-1	Area-2
PI	K_{Pi}	0.3027	0.2898	0.3022	0.2782
	K_{Ii}	0.4867	0.3823	0.4571	0.3678
PDFF	K_{Pi}	0.2972	0.2752	0.2875	0.2578
	K_{Ii}	0.4982	0.4634	0.4875	0.4123
	K_{FRI}	0.6521	0.6782	0.6478	0.5127
PIDF	K_{Pi}	0.4982	0.3117	0.4875	0.4431
	K_{Ii}	0.5783	0.4378	0.5127	0.5083
	K_{Di}	0.6012	0.5423	0.5478	0.5879
	N_i	20.478	19.578	10.234	15.278
FOPID	K_{Pi}	0.6458	0.7598	0.5978	0.6117
	K_{Ii}	0.7987	0.8782	0.6417	0.7248
	K_{Di}	0.9782	0.9745	0.6978	0.8759
	λ_i	0.8797	0.9762	0.7458	0.7589
	μ_i	0.5682	0.6457	0.4678	0.5789

Table 2. Comparative dynamic responses for different controller under Poolco based transactions.

Controller	Peak over/undershoot			Settling time in s		
	ΔF_1 in Hz	ΔF_2 in Hz	ΔP_{Tie12} in p.u.MW	ΔF_1	ΔF_2	ΔP_{Tie12}
PI	0.623	0.404	0.147	19.54	20.15	24.66
PDFF	0.509	0.245	0.116	13.87	14.79	15.48
PIDF	0.458	0.225	0.093	10.25	11.26	12.79
FOPID	0.368	0.166	0.077	9.247	10.52	11.25

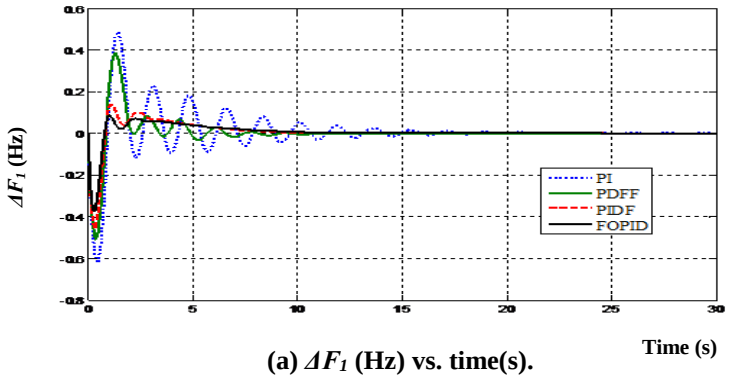

(a) ΔF_1 (Hz) vs. time(s).

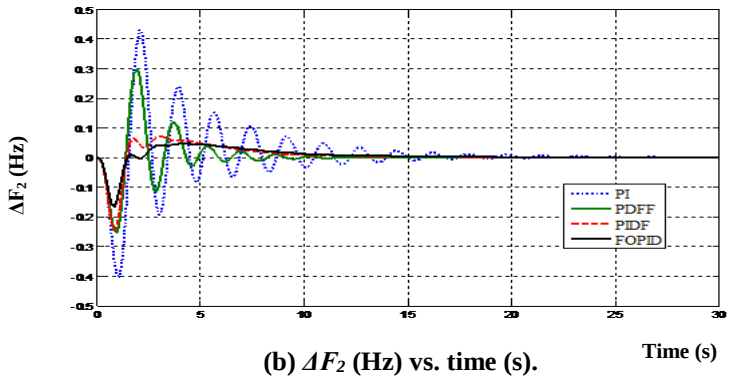

(b) ΔF_2 (Hz) vs. time (s).

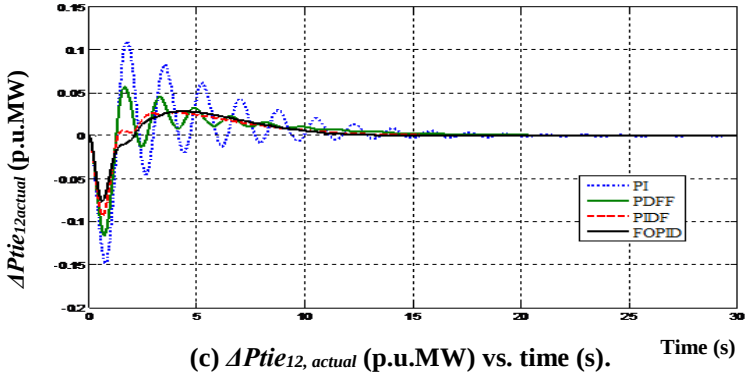

(c) $\Delta Ptie_{12,\ actual}$ (p.u.MW) vs. time (s).

Fig. 8. Dynamic responses of the frequency deviations, tie- line power deviations for a two-area wind-thermal system using different controller under Poolco based transactions.

Scenario 2. Bilateral based transactions

Here all the Discos have a contract with the Gencos and the following Disco Participation Matrix (DPM) referring to Eq. (1) is considered as:

$$DPM_2 = \begin{bmatrix} 0.2 & 0.3 & 0.1 & 0.4 \\ 0.3 & 0.2 & 0.3 & 0.1 \\ 0.25 & 0.1 & 0.25 & 0.3 \\ 0.25 & 0.4 & 0.35 & 0.2 \end{bmatrix} \tag{31}$$

In this case, the $Disco_1$, $Disco_2$, $Disco_3$ *and* $Disco_4$, demands of 0.1 pu.MW for each from Gencos as defined by *cpf* in the DPM_2 matrix and each Gencos participates in AGC as defined by the following ACE participation factor $apf_{11} = apf_{12} = 0.5$ and $apf_{21} = apf_{22} = 0.5$.

The optimal values of the corresponding controller's parameters are tabulated in Table 1 and the comparative dynamic responses are shown in Fig. 9. The corresponding peak over/undershoot and settling time of the system dynamic response are shown in Table 3.

From the results show that FOPID controller is performing improved in comparison to the rest of the controllers because of smaller peak variations and time to settle.

The main merit of FOPID controller has good stability for different transactions, excellent transient and dynamic responses in comparison with PI, PDFF and PIDF controllers. The above analysis revealed that FOPID controller has less peak deviation, the magnitude of oscillations, and faster settling time than others in all the transactions and shows superior performance for controlling of system oscillations.

Thus, FOPID can be used as a suitable secondary controller in both the AGC loop and the analysis of the succeeding sub-sections is continued by considering the same controller.

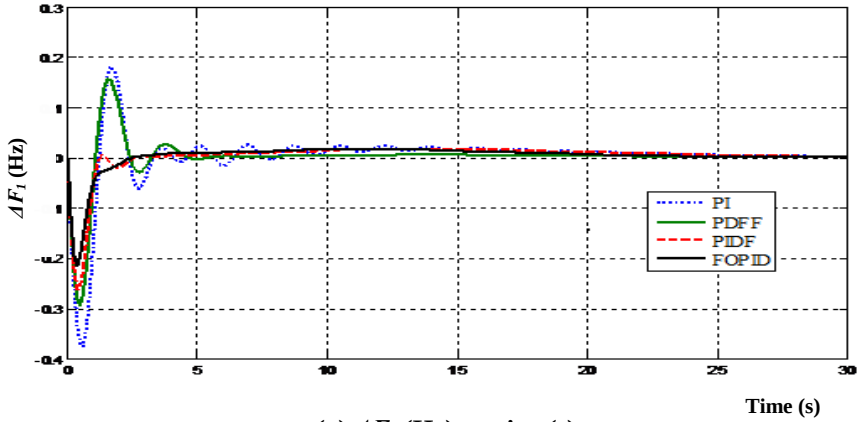

(a) ΔF_1 (Hz) vs. time(s).

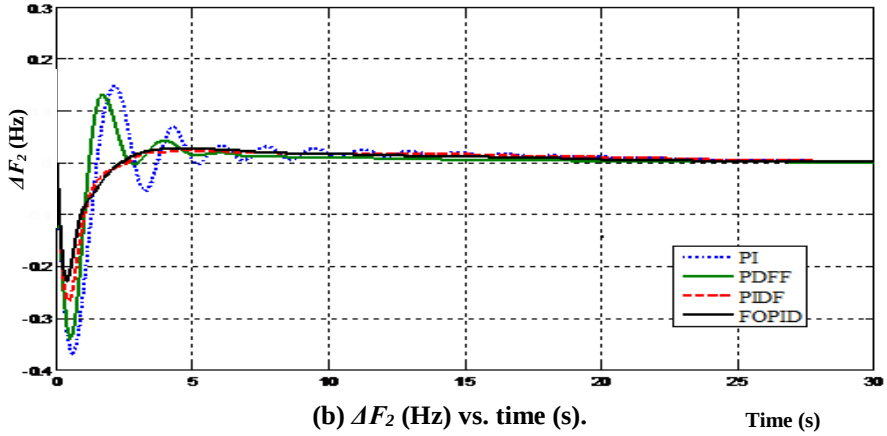

(b) ΔF_2 (Hz) vs. time (s).

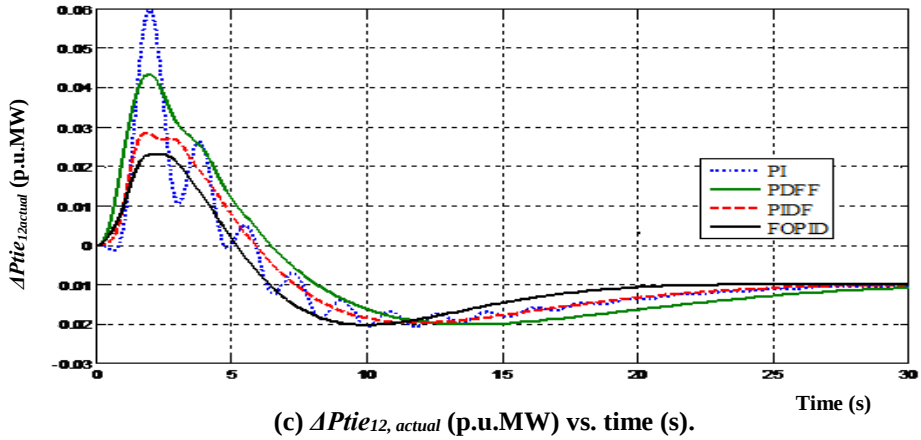

(c) $\Delta Ptie_{12,\ actual}$ (p.u.MW) vs. time (s).

Fig. 9. Dynamic responses of the frequency deviations, tie- line power deviations for a two-area wind-thermal system using different controller under Bilateral based transaction.

Table 3. Comparative dynamic responses for different controller under Bilateral based transactions.

Controller	Peak over/undershoot			Settling time in s		
	ΔF_1 in Hz	ΔF_2 in Hz	ΔP_{Tie12} in p.u.MW	ΔF_1	ΔF_2	ΔP_{Tie12}
PI	0.376	0.373	0.059	20.42	21.79	30.25
PDFF	0.293	0.341	0.043	19.23	20.48	29.18
PIDF	0.261	0.265	0.029	17.59	16.42	28.19
FOPID	0.213	0.229	0.022	11.55	15.48	26.46

5.2. Dynamic output responses of the AGC loop with IPFC and RFB units

In this Section, the effect of IPFC and RFB units are incorporated in the AGC loop for wind-thermal deregulated power system under bilateral transactions. The LSA optimized FOPID controller is considered for analysis of system performance. The gain value of RFB unit (K_{RFB}) is calculated using Eq. (26) for the given value of the speed regulation coefficient (R).

The purpose of utilizing IPFC unit is to damp out the peak value of frequency deviations in both areas and the tie-line power deviations. Since the system in Eq. (27) is second-order system, the peak overshoot *Mp* (new) can be specified in Table 4 and corresponding feedback gains k_1 and k_2 are found using Eq. (29).

The control parameters of RFB and IPFC units are shown in Table 4. The comparative transient performances of two-area wind-thermal deregulated power system with IPFC and RFB units using FOPID controller for the bilateral transactions are shown in Fig. 10 and it can be observed that the oscillations in area frequencies and tie-line power deviation have decreased to a considerable extent as compared to that of the system without RFB and IPFC units.

It may be concluded that the proposed design concept effectively damps out the inertia mode and inter-area mode because of the coordinated control action of RFB and IPFC units and are found to be more effective to suppress the frequency deviations of the two area system.

Table 4. Results obtained based on control design with IPFC and RFB units.

S. No.	System performance with R = 2.4 Hz/p.u. MW and RFB gain value by Eq. (26), K_{RFB} = 0.902
1	Eigenvalue of system without IPFC Eq. (27) $\lambda 1$ = - 0.25 +j 1.8081 $\lambda 2$ = - 0.25 - j 1.8081
2	Inter-area mode, without IPFC *Mp* = 64.85%
3	Design specification, with IPFC *Mp* (new =5 %)
4	New eigenvalue of the system with IPFC Eq. (27) $\lambda 1$ (new) = -1.724 + j1.8081 $\lambda 2$ (new) = -1.724 - j1.8081
5	State feedback gain value of IPFC Eq. (29) [K_1, K_2]= [-0.566, -0.908]

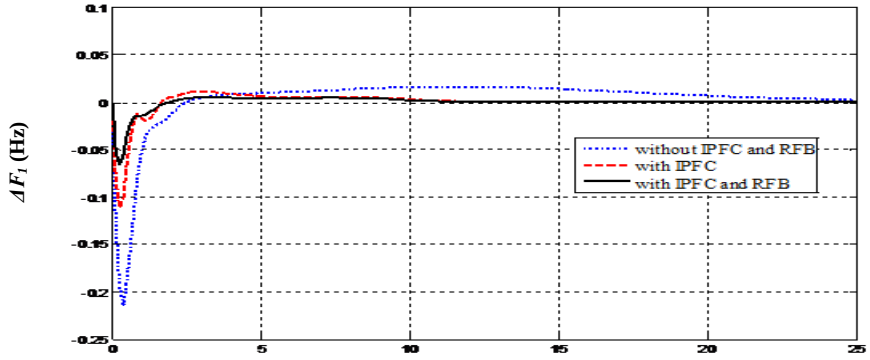

(a) ΔF_1 (Hz) vs. time(s).

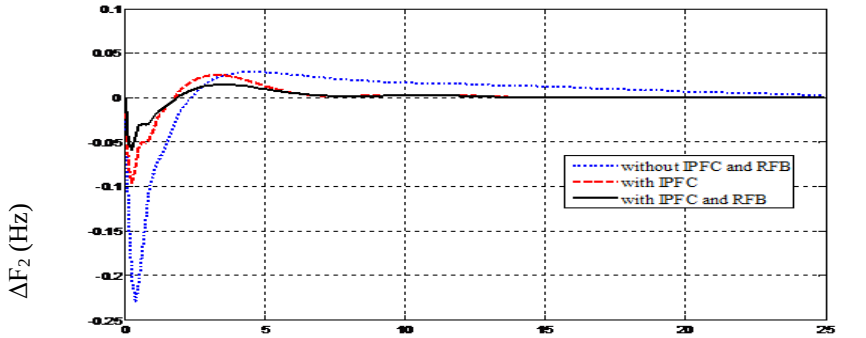

(b) ΔF_2 (Hz) vs. time (s).

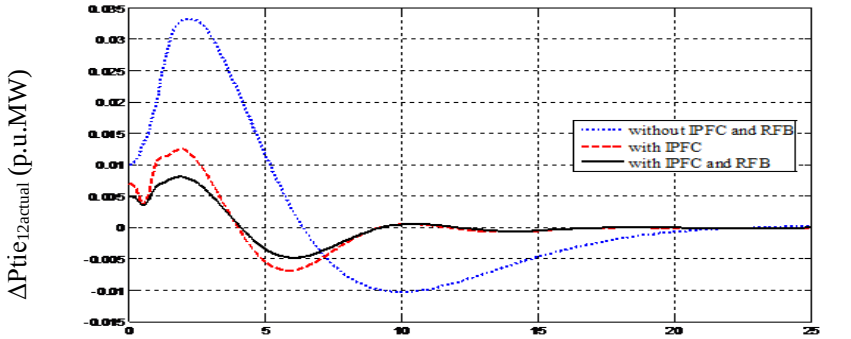

(c) $\Delta Ptie_{12,\ actual}$ (p.u.MW) vs. time (s).

Fig. 10. Dynamic responses of the frequency deviations, tie- line power deviations for a two-area wind-thermal system using FOPID controller with IPFC and RFB under Bilateral based transaction.

6. Conclusions

The proposed FOPID controllers are formulated to use Lightning Search Algorithm and realized in two-area interconnected wind-thermal deregulated

power system without and with RFB and IPFC units for different types of transactions. The superiority of the proposed LSA approach has been shown by comparing the results with PSO and BFO technique for the same interconnected power system. It is observed that the proposed LSA optimized FOPID controller outperforms the PSO and BFO optimized FOPID controller and the best performance is obtained with LSA optimized FOPID controller. Moreover, the various simulated results show that the LSA based FOPID controller's performance is swift, more accurate and better than the simulated results with PI, PDFF and PIDF controllers. In this study, it clearly reveals that FOPID controller is much better than Integral order controllers in enhancing system control performances. The coordinated application of RFB and IPFC units in the AGC loop is also very effective in settling frequency disturbances during bilateral and contract violation by the companies. Thus, the coordination of RFB-IPFC unit is effectively applied for stabilizing the load frequency issues in a two area wind-thermal system under the deregulated environment.

Nomenclatures

K_{Di}	Derivative feedback gain of area i
K_{Pi}	Proportional feedback gain of area i
K_{RFB}	Gain constant of Redox Flow Batteries
K_{Ii}	Integral feedback gain of area i
K_{pi}	Gain associated with transfer function of area, Hz/p.u. MW
N	Number of interconnected areas
P_{Ci}	Area speed changer output in p.u. MW
P_{Di}	Area real power load in p.u. MW
Pei	The total power exchange of area-I, p.u. MW/Hz
P_{Mi}	Mechanical (turbine) power output, p.u. MW
R	Steady state regulation of the governor, Hz/ p.u. MW
T_{RFB}	Time constant of the Redox Flow Batteries, s
T_{IPFC}	Time constant of the Interline Power Flow Controller, s
T_g	Steam turbine speed governor time constant, s
T_{ps}	Area time constant, s

Abbreviations

AGC	Automatic Generation Control
DISCO	Distribution companies
DPM	Disco Participation Matrix
FOPID	Fractional Order Proportional-Integral-Derivative controller
GENCO	Generation companies
IPFC	Interline Power Flow Controller
LSA	Lightning Search Algorithm
PDFF	Pseudo-Derivative Feedback with Feed-forward controller
PI	Proportional-Integral
PIDF	Proportional Integral Derivative with Filter controller
RFB	Redox Flow Batteries

References

1. Shankar, R.; Pradhan, S.R.; Chatterjee, K.; and Mandal, R. (2017). A comprehensive state of the art literature survey on LFC mechanism for power system. *Renewable and Sustainable Energy Reviews*, 76, 1185-1207.
2. Elgerd, O.I. (2016). *Electric energy systems theory: An introduction (2nd ed.)*. New Delhi, India: McGraw Hill Education (India).
3. Donde, V.; Pai, M.A.; and Hiskens, I.A. (2001). Simulation and optimization in an AGC system after deregulation. *IEEE Transactions on Power Systems*, 16(3), 481-489.
4. Nain, P.; Parmar, K.P.S.; and Singh, A.K. (2013). Automatic generation control of an interconnected power system before and after deregulation. *International Journal of Computer Applications*, 61(15), 11-16.
5. Pujara, S.M.; and Kotwal, C.D.; (2016). An inclusive review on load frequency control in deregulated market. *International Journal on Electrical Engineering and Informatics*, 8(3), 595-611.
6. Pappachen, A.; and Fathima, A.P. (2017). Critical research areas on load frequency control issues in a deregulated power system: A state-of-the-art-of-review. *Renewable and Sustainable Energy Reviews*, 72, 163-177.
7. Saha, D.; and Saikia, L.C. (2017). Performance of FACTS and energy storage devices in a multi area wind-hydro-thermal system employed with SFS optimized I-PDF controller. *Journal of Renewable and Sustainable Energy*, 9(2), 024103.
8. Hingorani, N.G.; and Gyugyi, L. (2000). *Understanding FACTS: Concepts and technology of flexible AC transmission systems*. New Jersey, United States of America: IEEE Press Marketing.
9. Gorripotu, T.S.; Sahu, R.K.; and Panda, S. (2015). AGC of a multi-area power system under deregulated environment using redox flow batteries and interline power flow controller. *Engineering Science and Technology, an International Journal*, 18(4), 555-578.
10. Chidambaram, I.A.; and Paramasivam, B.; (2012). Control performance standards based load-frequency controller considering redox flow batteries coordinate with interline power flow controller. *Journal of Power Sources*, 219, 292-304.
11. Sasaki, T.; Kadoya, T.; and Enomoto, K. (2004). Study on load frequency control using redox flow batteries. *IEEE Transactions on Power Systems*, 19(1), 660-667.
12. Saikia, L.C.; and Sahu, S.K. (2013). Automatic generation control of a combined cycle gas turbine plant with classical controllers using firefly algorithm. *International Journal of Electrical Power and Energy Systems*, 53, 27-33.
13. Sahu, R.K.; Panda, S.; and Padhan, S. (2014). Optimal gravitational search algorithm for automatic generation control of interconnected power systems. *Ain Shams Engineering Journal*, 5(3), 721-733.
14. Wei, Y.-H; Sun, Z.-Y.; Hu, Y.-S.; and Wang, Y. (2015). On fractional order adaptive observer. *International Journal of Automation and Computing*, 12(6), 664-670.

15. Sondhi, S.; and Hote, Y.V. (2014). Fractional order PID controller for load frequency control. *Energy Conversion and Management*, 85, 343-353.
16. Alomoush, M.I. (2010). Load frequency control and automatic generation control using fractional-order controllers. *Electrical Engineering*, 91(7), 357-368.
17. Bhatt, P.; Roy, R.; and Ghoshal, S.P. (2010). GA/particle swarm intelligence based optimization of two specific varieties of controller devices applied to two-area multi-units automatic generation control. *International Journal of Electrical Power and Energy Systems*, 32(4), 299-310.
18. Nanda, J.; Mishra, S.; and Saikia, L.C. (2009). Maiden application of bacterial foraging-based optimization technique in multi area automatic generation control. *IEEE Transactions on Power Systems*, 24(2), 602-609.
19. Gozde, H.; and Taplamacioglu, M.C. (2011). Automatic generation control application with craziness based particle swarm optimization in a thermal power system. *International Journal of Electrical Power and Energy Systems*, 33(1), 8-16.
20. Chatterjee, S.; and Mukherjee, V. (2016). PID controller for automatic voltage regulator using teaching-learning based optimization technique. *International Journal of Electrical Power and Energy Systems*, 77, 418-429.
21. Kumar, N.; Kumar, V.; and Tyagi, B. (2016). Optimization of PID parameters using BBBC for a multi area AGC scheme in a deregulated power system. *Turkish Journal of Electrical Engineering and Computer Sciences*, 24(5), 4105-4116.
22. Chandrasekar, K.; Paramasivam, B.; and Chidambaram, I.A. (2017). Evaluation of power system restoration indices using krill herd algorithm based optimized pi+ controller for a restructured power system with facts devices. *ARPN Journal of Engineering and Applied Sciences*, 12(17), 4973-4989.
23. Shareef, H.; Ibrahim, A.A.; and Mutlag, A.H. (2015). Lightning search algorithm. *Applied Soft Computing*, 36, 315-333.
24. Rajbongshi, R.; and Saikia, L.C. (2017). Combined control of voltage and frequency of multi-area multisource system incorporating solar thermal power plant using LSA optimised classical controllers. *IET Generation, Transmission and Distribution*, 11(10), 2489-2498.

Appendix A

Data for the Interconnected Two-Areas Interconnected Power System [7, 10]

Rating of each area = 2000 MW, Base power = 2000 MVA, f = 60 Hz, $R_1 = R_2 = R_3 = R_4$ = 2.4 Hz/p.u.MW, $K_{p1} = K_{p2}$ = 120Hz/p.u.MW, $T_{p1} = \underline{T_{p2}}$ = 20 s, $\beta_1 = \beta_2$ = 0.425 p.u.MW/Hz, Thermal unit: T_{gi} = 0.08 s, T_{ti} = 0.3 s, K_{ri} = 5,T_{ri} = 10 s; Wind unit: WPP: K_{wp1} = 1.25, T_{wp1} = 6 s, K_{wp2} = 1.4, T_{wp1} = 0.041 s $2\pi T_{12}$ = 0.545 p.u.MW/Hz, a_{12} = -1, IPFC unit: T_{IPFC} = 0.01 s, RFB unit: T_{RFB} = 0.